PFC/JA-88-16

H_α Laser Fluorescence Diagnostic on the Tara Tandem Mirror Experiment

Guss, W.C.; †Yao, X.Z.; ‡Pócs, L.;
§Mahon, R.; Casey, J.; and Post, R.S.

April, 1988

Plasma Fusion Center
Massachusetts Institute of Technology
Cambridge, MA 02139

Submitted for publication in Review of Scientific Instruments

† Permanent Address: Institute of Physics, Beijing, China

‡ Permanent Address: Central Research Institute of Physics, Budapest, Hungary

§ Permanent Address: Laser Physics Branch, Code 6540, Naval Research Laboratory, Washington, DC 20375

H_α Laser Fluorescence Diagnostic on the Tara Tandem Mirror Experiment

W.C. Guss, X.Z. Yao†, L. Pócs‡,
R Mahon§, J. Casey, and R.S. Post

Plasma Fusion Center, MIT

Abstract

A laser fluorescence diagnostic has been used for measuring the neutral hydrogen density in the central cell of the Tara thermal barrier tandem mirror. Experiments have been performed using laser-induced, resonance fluorescence detection of H_α $(6563\mathring{A})$ radiation. Measurements were made at a number of radial positions with 1 cm resolution, from the magnetic axis to near the plasma limiter. Stray laser light contributions to the signal were eliminated with a double pulse technique. For comparison, the chord-averaged plasma H_α radiation was analyzed under the identical conditions for which laser fluorescence data were taken.

Introduction

Characterizing the neutral gas evolution in Tara was the goal of a program of extensive spectroscopic studies which included passive line-of-sight studies and laser induced resonance fluorescence measurements. Measuring the H_α laser-fluorescence scattering from a plasma is a means of determining the neutral hydrogen density with both spatial and temporal resolution[1]. In addition to being one of the few methods available for determining the neutral density, it is nonperturbing and, when combined with independently measured electron temperature and densities, yields an absolute result. This method has been applied to toroidal plasmas for the study of fuel[2,3,4] and impurity evolution[5,6,7].

Laser Fluorescence System

A portion of the central cell of Tara is shown in Fig. 1. The fueling in Tara is provided by a gas box[8] located near the middle of the central cell and near the top of a local magnetic field maximum (R=2). As a result of the field bump, two magnetic 'wells' are defined in the central cell, each approximately half the central cell in length. Neutral hydrogen gas flowing out of the gas box must pass through a nearby ICH resonance where it has a high probability of being ionized. As a result, the bulk of the plasma volume is isolated from neutral gas and the resulting charge exchange losses.

The fluorescence diagnostic consisted of a tunable, flashlamp-pumped dye laser (Candela EDL-6), beam steering optics, detection optics, and both a beam dump and a viewing dump (Fig. 2, 3). The diagnostic location at 174 cm is well outside the gas box which extends to about 50 cm. The 30 cm x 10 cm viewing dump was made of stacked non-magnetic razor material and was located on the opposite wall of the diagnostic box, but symmetric to, the viewing window. The viewing optics were chosen to image a 2.5 cm diameter disc in the center plane of the diagnostic box. Since the laser beam was 1 cm in diameter the actual scattering volume was 2.5 cm^3 and an emitting area of ≈ 2 cm^2. The laser was tuned to the Balmer-alpha line at 6563 $\AA$ with an angle-tuned 40 μm air-spaced etalon, giving a linewidth of about 0.75 $\AA$ which allowed scattering from both the .4 and 4 eV Franck-Condon neutral components. A high resolution Ebert monochromator[9] was used to monitor the wavelength of the laser output.

The laser pulse duration was 5μsec, being long enough to give an improved signal to noise level and yet short enough to give adequate temporal

resolution. Radial scans were restricted in extent to $r = 15$ cm because of the sizes of both the viewing dump and the large aperture collection lens. This is to be compared with the limiter radial width of 22.5 cm and a typical plasma radial scale length of $11 - 13$ cm. The plasma was scanned radially by translating the 7 cm diameter, 10 cm focal length collection lens across a permanently mounted 30 cm x 10 cm observation window. A flapper unit protected the observation window from nearby Ti gettering sources; it being opened only during the plasma shot. Three copper knife-edge baffles were arranged both directly behind the laser input window and before the beam dump in order to minimize the stray light level. The beam dump consisted of two discs of absorbing OB10 type glass, set at Brewster's angle to the incident laser direction, in such a way that both polarization components were attenuated. The scattered signal was relayed to a magnetically shielded Hamamatsu R928 photomultiplier tube via a 250 cm length quartz fiber bundle, with a transmission of 50%. A narrow band interference filter, having a bandpass of $5\mathring{A}$ and a transmission of 53%, was placed in a region of collimated light in front of the photomultiplier tube, thereby reducing the plasma background contribution to the scattered signal. The photomultiplier output was amplified by a factor of 10 before being processed in a 150 MHz digitizer. The laser power of $1 - 10$ kWcm$^{-2}\mathring{A}^{-1}$ was sufficient to saturate the $n = 2$ to $n = 3$ transition so that the fluorescence was not dependent on the actual value, or on any small fluctuation in, the laser intensity. A photodiode, mounted directly behind the 99.9% reflecting rear mirror of the dye laser, was used to continuously monitor each laser pulse.

The residual problems associated with stray laser light were overcome by using a double pulse technique. A typical laser fluorescence data set for a plasma discharge in Tara is shown in Fig. 4. The stray light level was measured during a laser pulse fired 2-3 sec prior to the plasma discharge. A second laser pulse, at a known time during the discharge, contained the stray laser light, together with the plasma background and the resonance laser fluorescence signals. The difference of the signals above the plasma background level, normalized to the laser power, yielded the desired H_α fluorescence signal. Data was accumulated on a shot by shot basis since only one temporal and spatial point are taken per discharge.

Absolute calibration was made using Rayleigh scattering in nitrogen up at a few hundred Torr. In this way the measurements did not depend on having to know the actual collection solid angle or efficiency for detection,

or the gain of the photomultiplier. For a fluorescence signal level F, and a corresponding Rayleigh scattered signal R,

$$\frac{F}{R} = \frac{DN_3\ A_{32}\ T_L\ \pi r^2}{N_L\ N_{N2}\ \sigma_R}$$

where N_3^{laser} is the saturated population in the n=3 level, N_3^0 is the population in the absence of laser irradiation, and DN_3=N_3^{laser}-N_3^0. A_{32} is the induced transition probability and equals 4.4×10^7 sec^{-1}. T_L=5 μsec, is the duration of the saturated fluorescence signal, and πr^2 is the area of the laser beam in the plasma scattering volume. N_L is the number of photons in the laser beam which contribute to the Rayleigh scattered signal. Different polarization contributions need to be taken into account and any differences in bandwidth of the laser in excess of that which contributes to the fluorescence signal. N_{N2} is the molecular nitrogen number density in the Rayleigh scattering. Finally, the Rayleigh scattering cross section σ_R = 2.16×10^{-27} cm^2. Experimentally, the Rayleigh scattered signal was found to be R=5.5p, with p being measured in Torr.

In order to relate DN_3 to the ground state population the electron density and temperature were measured using Thomson scattering of ruby laser light. These measurements were made nearby (z = 330 cm) on the same flux surface and during the same discharge as the laser fluorescence measurements. For the experimental range of T_e, the data analysis was nearly independent of the assumed T_e.

Typical data are shown in Fig. 5 The electron density profile decreases monotonically toward the edge from a central value of $\approx 3 \times 10^{12}$ cm^{-3} on the magnetic axis. From a four chord interferometer array, the profile is best fit with a Gaussian with a 12−13 cm scale length. The electron temperature profile increases from $\approx$ 70 eV on axis to $\approx$ 110 eV at the edge, presumably because of the strong edge electron heating from the central cell ICH.

Results

The ground state population of the neutral hydrogen atoms is inferred from the measured n=2 population using the collisional-radiative model of Gohil and Burgess[10]. Radial profiles of the hydrogen density were recorded at two times during the plasma discharge. The first was at 8 ms after the ICH at which time the axial H_α signal was no longer changing. The edge pressure was still dropping at this early time. For these discharges, the

neutral density profile was hollow (Fig. 5) with the on-axis density about an order of magnitude down from the edge ($r = 15$ cm) density. The profile could be approximated by an edge section with short radial scale length (≈ 2 cm) and by a central section with a longer scale length on the order of, or larger than, the plasma radius itself. The short scale length was consistent with room temperature neutrals penetrating a plasma with $T_e = 80$ eV and $n_e = .5 \times 10^{12}$ cm^{-3}. Neutrals with energy above ≈ 1 eV were consistent with the longer central scale length. At the largest radial extent of the laser fluorescence, the fraction of neutrals was 2%. On the magnetic axis the fraction was .04%. Fast ionization gauges imply a molecular density behind the limiter of about 2×10^{11} cm^{-3} ($r \geq r_p = 22.5$ cm) while the neutral atomic density at the plasma edge was $\approx 1 \times 10^{10}$ cm^{-3} ($r = 15$ cm) as deduced from the laser fluorescence scattering results.

Background H_α light (Fig. 4) contains recognizable low frequency (≈ 25 kHz) fluctuations. The radial distribution of the fluctuation amplitude is shown in Fig. 6. Microwave interferometers observe similar fluctuations of the electron density which could be responsible for the light variations. Large edge density fluctuations would explain the large edge H_α fluctuations. It does not however explain the coincidence of the gradient location for both the neutral density and the plasma fluctuations.

Data was also taken at a second time, 20 ms, when both the axial H_α and the edge pressure were in steady state. The edge molecular density was somewhat lower (6×10^{10} cm^{-3}). As at the earlier time, the edge radial scale length was short (≈ 3 cm), with a near constant neutral density towards the magnetic axis. The central and edge atomic hydrogen density were about the same as at the earlier time. From the two radial scans it appeared that the profile was constant while the edge pressure was constant. The on-axis neutral density time history is shown in Fig. 7 and compared to the axial H_α. It extends over a larger time span than the two radial profiles and also shows a relatively constant density during the discharge. It is similar to the axial H_α trace with an initial peak and a roughly constant lower level.

As a comparison, the chord-averaged plasma H_α was analyzed. For the same discharges that the laser fluorescence data was taken, the H_α intensity was fit with a polynomial and Abel inverted. To eliminate the electron density contribution to the light intensity, the inverted data was normalized to a Gaussian radial profile and is shown in Fig.8 compared to the laser fluorescence profile. The resulting curve is proportional to the

product of the neutral density and the excitation rate. The two curves have similar shape with some divergence toward larger radii. The light intensity curve being somewhat lower is consistent with the electron temperature decreasing toward the edge. This is also where the electron temperature measurement is least certain. The edge to center intensity ratio, and the inferred neutral ratio, is about 30% of the laser fluorescence measured ratio.

Acknowledgment

This work was supported by U.S. DOE Contract No. DE-AC02-78ET5101

†Permanent Address: Institute of Physics, Beijing, China

‡Permanent Address: Central Research Institute of Physics, Budapest, Hungary

§Permanent Address: Laser Physics Branch, Code 6540, Naval Research Laboratory, Washington, D.C. 20375

References:

[1]V.S. Burakov, P. Ya. Misyakov, P.A. Naumenko, S.V. Nechaev, G.T. Razdobarin, V.V. Semenov, L.V. Sokolova, and I.P. Folomkin, JETP Lett. **26**, 403(1977)

[2]P. Bogen and E. Hintz, Comm. Plasma Phys. Contr. Fusion **4**, 115(1978)

[3]P. Bogen, R.W. Dreyfus, Y.T. Lie, and H. Langer, J. Nucl. Materials **111**, 75 (1982)

[4]P. Gohil, G. Kolbe, M.J. Forrest, D.D. Burgess, and B.Z. Hu, J. Phys. **D 16**, 333(1983)

[5]B. Schweer, D. Rusbueldt, E. Hintz, J.B. Roberto, and W.R. Husinsky, J. Nucl. Mater. **93**, 357(1980)

[6]C.H. Muller, and K.H. Burrell, Phys. Rev. Lett. **47**, 330(1981)

[7]B. Reinhold, J. Hackman, and J. Uhlenbusch, J. Nucl. Mater. **121**, 231(1984)

[8]R.S. Post, K. Brau, S. Golovato, E. Sevillano, D.K. Smith, W. Guss, J. Irby, R. Myer, and J. Sullivan, Nucl. Fusion **27**, 217(1987)

[9]M.B. Morris, and T.J. McIlrath, Applied Optics, **18**, 4145(1979)

[10]P. Gohil, and D.D. Burgess, Plasma Phys. **25**, 1149(1983), and by private communication with P. Gohil, G.A. Technologies Inc.

Figure Captions:

FIG. 1. Tara central cell and axial magnetic field with ICH slot antenna and gas box. The laser fluorescence diagnostic is 140 cm from the midplane.

FIG. 2. Laser fluorescence optical bench arrangement showing alignment laser and monochromator for monitoring dye-laser wavelength.

FIG. 3. Laser beam collimation and beam dump with viewing optics and viewing dump.

FIG. 4. Typical data set for a Tara discharge. The top row contains the laser monitor signals during (a) and after (b) the plasma pulse. The bottom row shows the detector signal for the laser scattered light during the plasma (c), and for the fluorescence plus scattered light after the plasma (d).

FIG. 5. Radial profiles of laser fluorescence inferred n_o (a), which was reduced from the raw Fluorescence data (b), using the Thomson scattering T_e (c), and n_e (d).

FIG. 6. Radial distribution of the fluctuations in the background H_α detected by the laser fluorescence diagnostic.

FIG. 7. Time history of the laser fluorescence measured atomic density on axis, and the line integrated core H_α taken along the entire length of the machine.

FIG. 8. The laser fluorescence neutral density at 8 ms is compared to the Abel inverted H_α signal normalized to a Gaussian electron density profile.

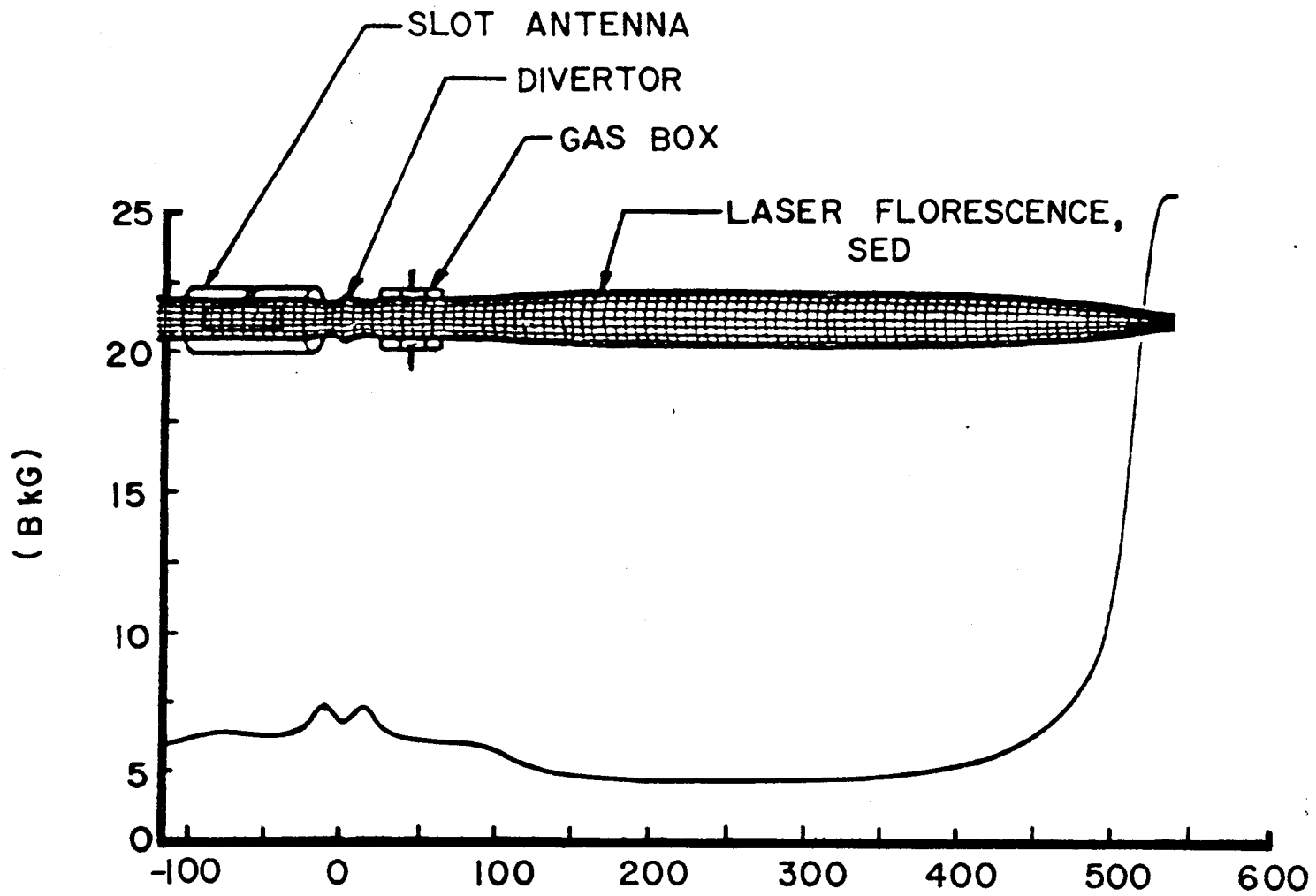
SLOT ANTENNA
DIVERTOR
GAS BOX
LASER FLORESCENCE, SED
25
20
15
10
5
0
(B kG)
-100
0
100
200
300
400
500
600
Z (CM)
TARA AXIAL MAGNETIC

Figure 1

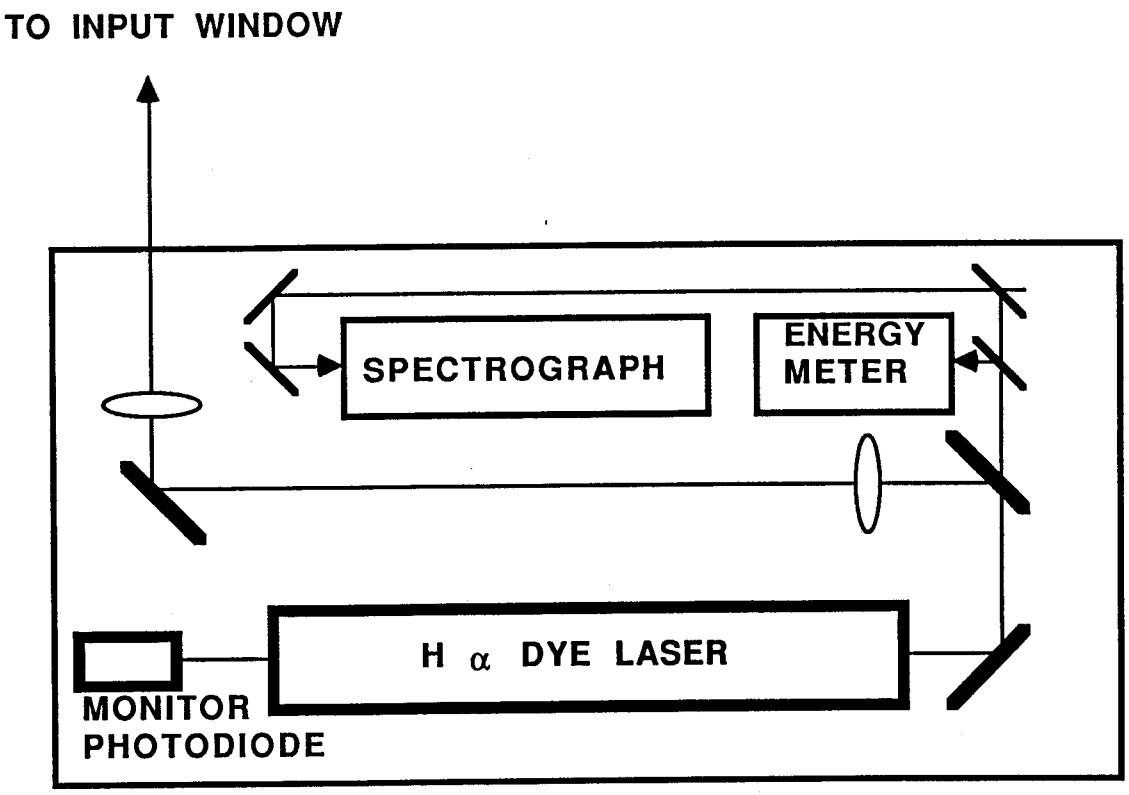
TO INPUT WINDOW
SPECTROGRAPH
ENERGY METER
H α DYE LASER
MONITOR PHOTODIODE

Figure 2

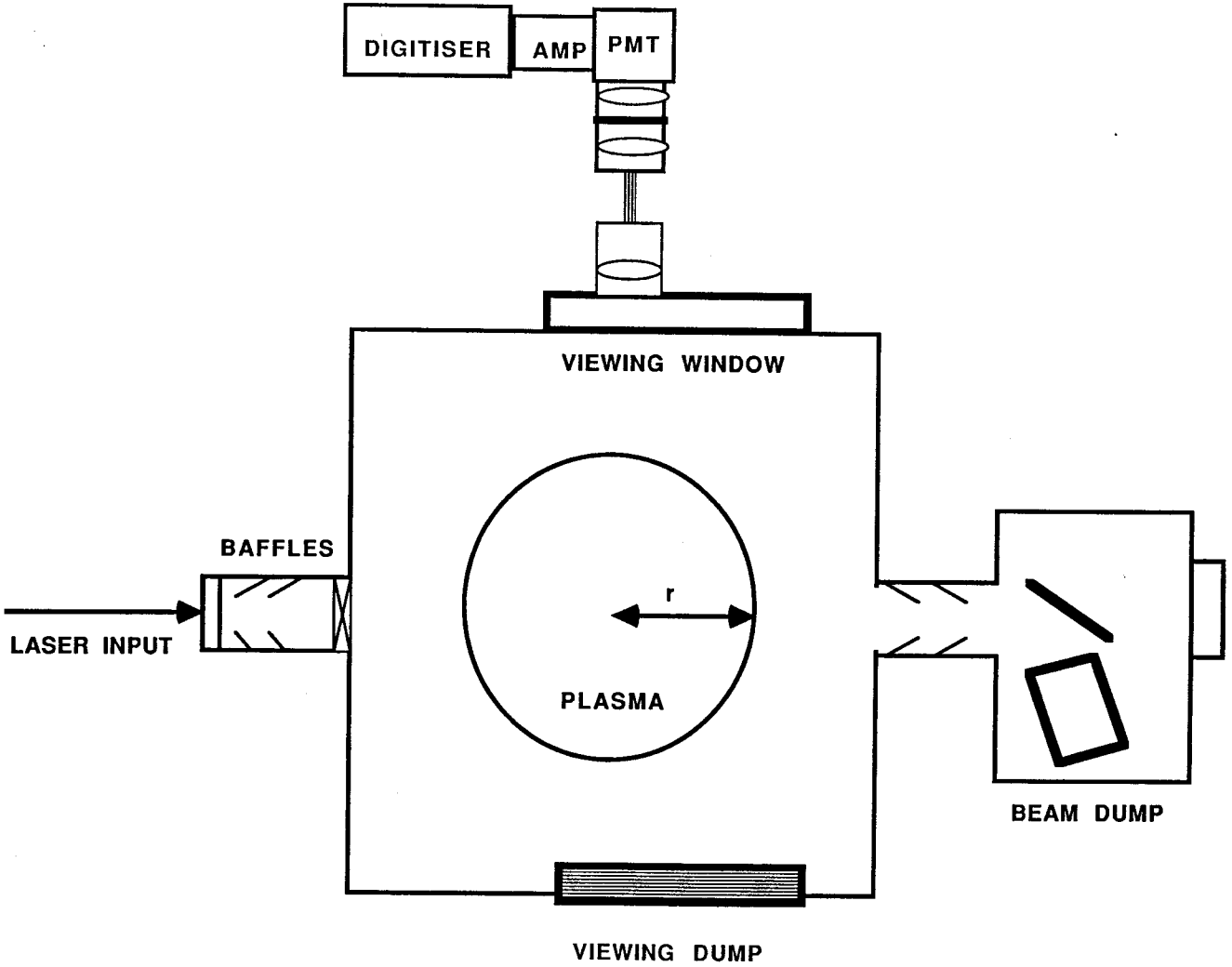
DIGITISER
AMP
PMT
VIEWING WINDOW
BAFFLES
LASER INPUT
r
PLASMA
BEAM DUMP
VIEWING DUMP

Figure 3

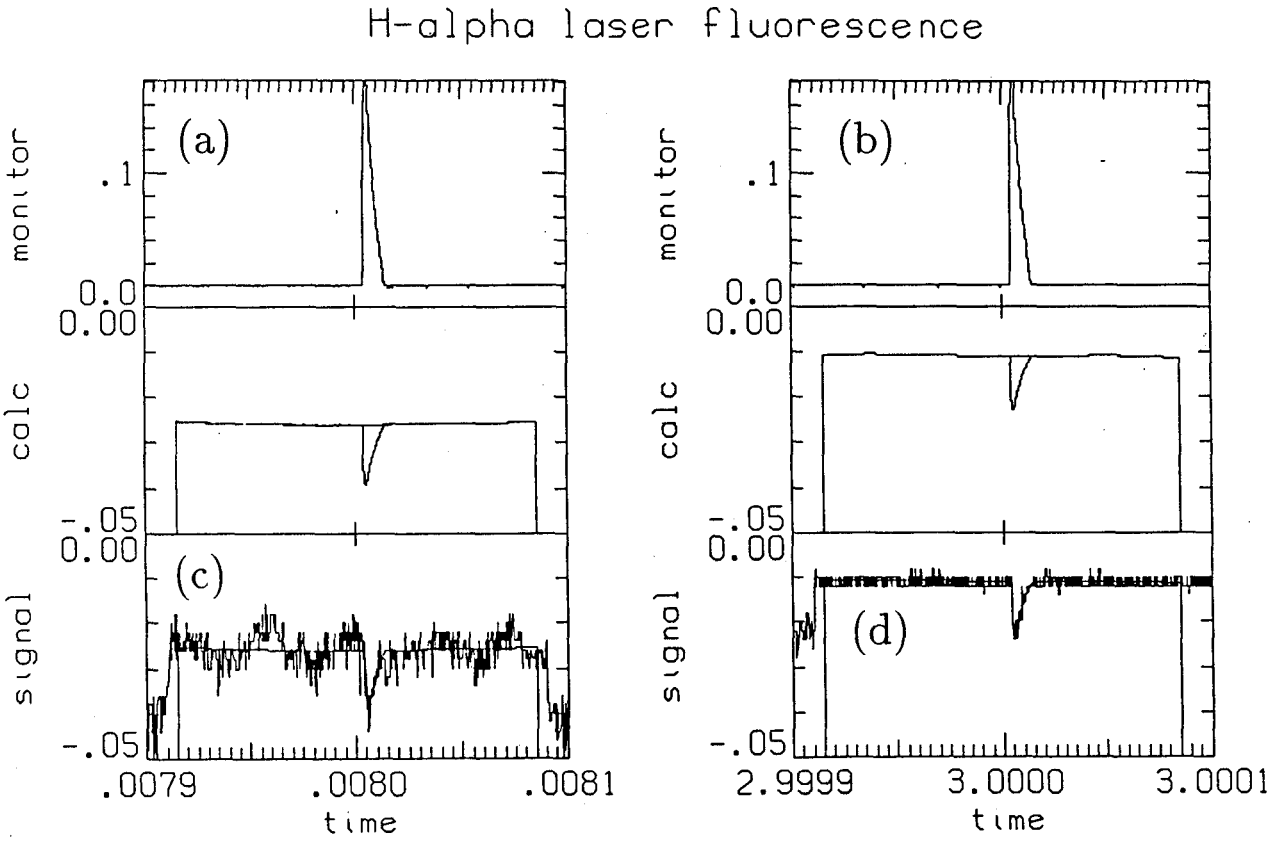
H-alpha laser fluorescence
monitor
.1
0.0
(a)
(b)
0.00
calc
-.05
0.00
signal
(c)
(d)
-.05
.0079
.0080
.0081
time
2.9999
3.0000
3.0001
time

Figure 4

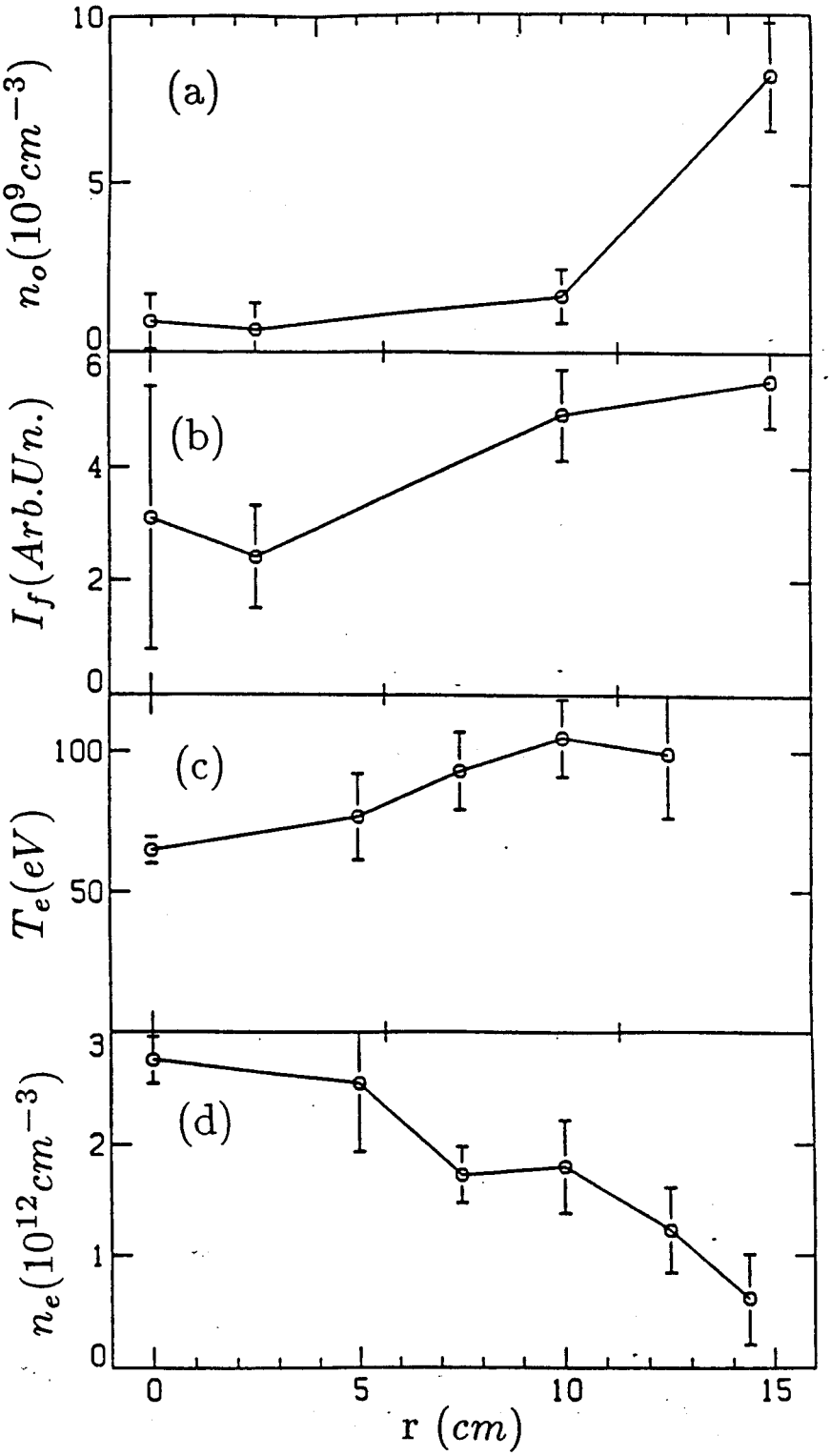

Figure 5

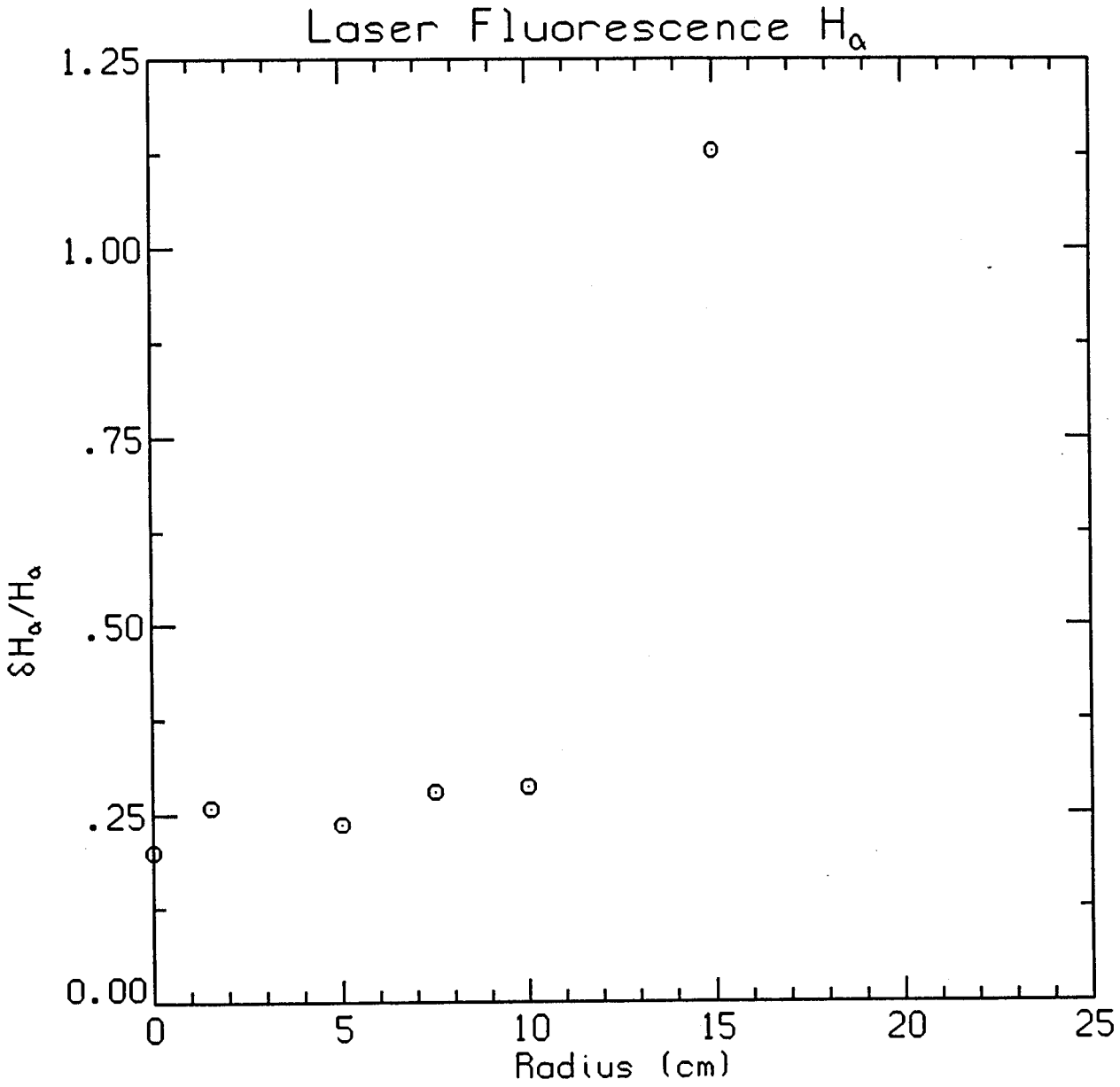
Laser Fluorescence H_α
1.25
1.00
.75
.50
.25
0.00
$\delta H_\alpha / H_\alpha$
0
5
10
15
20
25
Radius (cm)

Figure 6

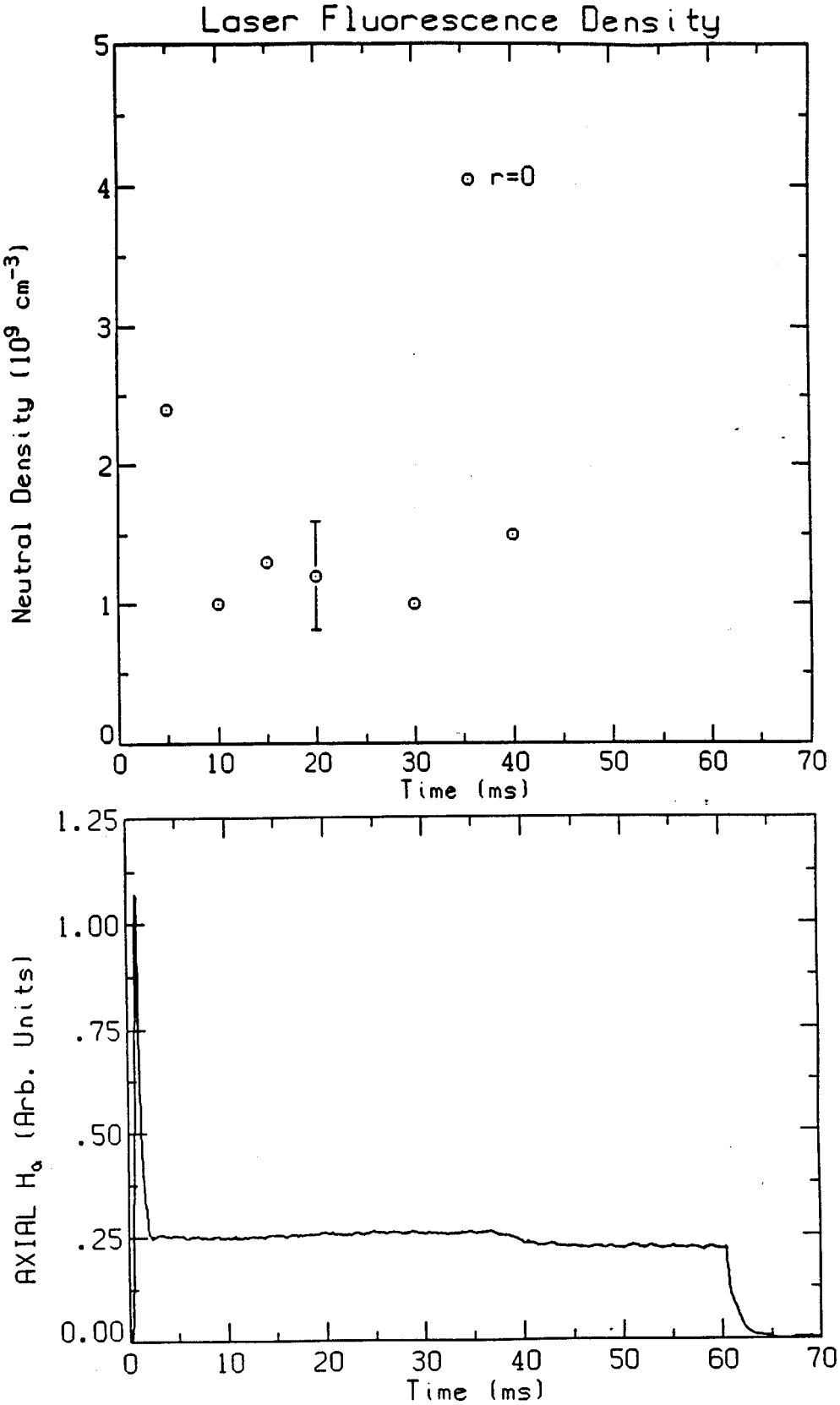
Laser Fluorescence Density
Neutral Density (10^9 cm^{-3})
r=0
Time (ms)
AXIAL H_α (Arb. Units)
Time (ms)

Figure 7

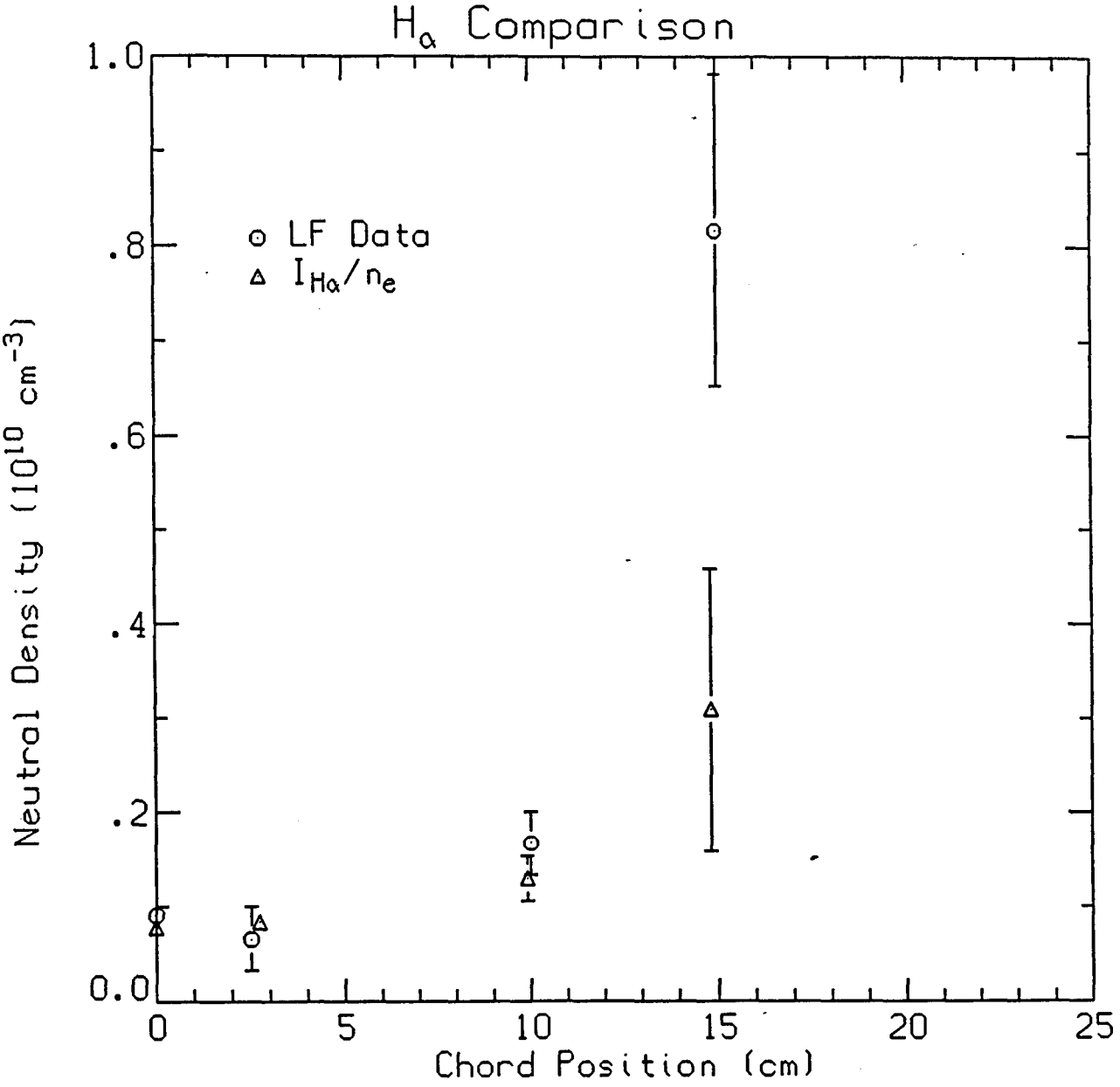
H_α Comparison
LF Data
$I_{H\alpha}/n_e$
Neutral Density (10^{10} cm^{-3})
1.0
.8
.6
.4
.2
0.0
0
5
10
15
20
25
Chord Position (cm)

Figure 8